

We are IntechOpen, the world's leading publisher of Open Access books Built by scientists, for scientists

6,900

Open access books available

186,000

International authors and editors

200M

Downloads

Our authors are among the

154

Countries delivered to

TOP 1%

most cited scientists

12.2%

Contributors from top 500 universities



WEB OF SCIENCE™

Selection of our books indexed in the Book Citation Index
in Web of Science™ Core Collection (BKCI)

Interested in publishing with us?
Contact book.department@intechopen.com

Numbers displayed above are based on latest data collected.
For more information visit www.intechopen.com



Analytical and Experimental Research of Machine Tool Accuracy

Peter Demeč and Tomáš Stejskal

Abstract

In this chapter, one of the ways of modelling the working accuracy of machine tools is elaborated. The method of constructing a numerical model based on transmission matrices is applicable in the field of virtual prototyping of modern machine tools. The results of numerical simulation of working precision are closely related to the machine stiffness in the machine workspace. A new way of measuring static stiffness can support numerical simulation results. Measurement of static stiffness is based on the measurement of the positioning accuracy of machine tools. The difference of the method lies in the load of the measured axis during the measurement. In this way, the stiffness of the movable machine partly relative to the base can be determined. The method for measuring static stiffness can advantageously be used in the development of new machine designs.

Keywords: machine tool, virtual prototyping, virtual machining, numerical experiment, static stiffness measurement

1. Introduction

Reducing the development time of modern machines is still a topical issue. Manufacturing experience is not sufficient to predict the characteristics of the machines being developed. Many solutions have to be tested and subsequently modified. This process requires experience but mainly time and cost. Computational technology in the form of virtual prototyping brings considerable acceleration of developing process. In addition to static parameters, the dynamic parameters of a virtual machine tool are now well verified. At the end of the development, a real machine tool is verified, which already requires considerably less modifications, as it was produced based on virtual testing of the virtual machine. Of course it is not possible to verify all the properties, but the system of virtual prototyping is constantly improving and expanding. This trend is confirmed by world trade fairs for machine tools (EMO). More and more sophisticated products supporting virtual prototyping are emerging on the market. Prototyping on the principle of virtual machining is a progressive direction. This type of analysis better simulates real production conditions and thus tests the designed machine using implemented mathematical models.

In this chapter, the practical application of virtual machining for virtual prototyping of machine tools will be explained, supplemented by the measurement of static stiffness of the machine tool. Typical sources of working inaccuracy are

kinematic errors, thermo-mechanical errors, static and dynamic loads [1], a motion control method and control software [2]. In addition, the working inaccuracy is also determined by the appropriate choice of technological conditions and the required power performance.

The issue of dynamic software adaptation of Tool Center Point (TCP) is addressed [3]. In many works [4–8], the main influence on the TCP position has to do with the temperature factor. Stiffness experiments have shown that besides temperature, the clearance and the manifestation of contact stiffness between bearings and ball screw also play an important role in precision.

The stiffness of the machine tool has a significant influence on the accuracy of its work. Machine tools with a serial cinematic structure are working on the principle that the resulting relative movement of the tool and the workpiece is required to change the shape and dimensions of the workpiece and the results of the superposition of the individual machine nodes. Several mathematical and experimental methods are used to determine this stiffness. Consequently, many works deal with the calculation of stiffness by the finite element method [9, 10].

The classical static stiffness measurement is performed on a stationary machine most often at the tool clamping point relative to the workpiece clamping point. The load jig is gradually loaded and the working area subsequently uploaded in the direction of the machine axes. The deflection gauge measures the deformation at a given point in the load direction. Based on the measured values, the stiffness at the place location is determined. At the same time, deflections are also measured outside the load location. This determines the contribution of deflections to the stiffness change from individual machine components. Such measurement has great importance in prototype testing. Measurement of stiffness contributions reveals machine design imperfections. Some parts need to be redesigned to increase their stiffness. This achieves an acceptable machine stiffness. Normally stiffness measurements are rarely performed in in-process inspection.

The actual position of the moving part of the machine tool in relation to its base, even under static load, is influenced by three basic nonlinearities. These are friction, backlash and compliance [7].

The aim of this work is to design experimentally verified mathematical models that will significantly streamline, shorten and improve the quality of the work of the constituents. The aim of this chapter was to verify experimentally static stiffness using an interferometer, which opens new possibilities of evaluation. Interferometer measurement is used to evaluate positioning accuracy under the not loaded machine. The proposed stiffness measurement methodology with the use of an interferometer opens up new effects of the individual system pulses on the overall accuracy of the machine work. However, there are many nonlinear elements in this field, so the construction of a reliable mathematical model is considerably limited.

2. Theoretical fundamentals

The relative movement of the tool is determined by contributions from all parts of the kinematic chain. This kinematic chain is generally made up of serially connected machine components from the cutting tool to the workpiece holder. The relative movement between the tool and the workpiece is given by the precision of the kinematic components, the force deformations of the components and the random values that result from the nonlinear elements. The simplest solution for virtual motion is based on the kinematic motion of rigid components. The executive elements are characterised by nodes that can perform rotational or translational

movement. In this way, the so-called ideal machined surface can be modelled. The surface is created as a trace of the ideal toolpath given by mathematical models.

To derive the mathematical model of the ideal tool trajectory, we will accept the following presumptions:

1. The relative movements of the machine's executive members will be examined as relative movements of the Cartesian coordinate systems linked with the workpiece, the individual executive members of the machine and its stationary nodes (e.g., the bed). All moving and stationary machine nodes involved in generating the resulting relative movement of the tool and workpiece will be called common how to model bodies.
2. The workpiece will have index 0, and its coordinate system $S_0 (O_0, X_0, Y_0, Z_0)$ will be considered as stationary in the space.
3. For each of the model bodies, we assign the index $i \in \langle 1; n \rangle$, where index 1 will have the model body immediately next to the workpiece and index n will have the model body that is the tool carrier. For other model bodies, we assign the increasing indexes in the direction from the workpiece to the tool.
4. The individual model bodies T_i will have the coordinate system $S_i (O_i, X_i, Y_i, Z_i)$, whose axes are in the starting position (i.e., to the beginning of the machining), parallel to the corresponding coordinate axes of the workpiece ($X_i || X_0, Y_i || Y_0, Z_i || Z_0$).
5. Model bodies can either stationary or can perform translational, respectively, rotational movement. One model body can perform only one of these movements and only in direction, respectively, around one coordinate axis of the previous model body.
6. The movements of all model bodies will follow the workpiece coordinate system.

Under these rules it is possible to derive relatively simple formulas for general application defining the position of any point $A \equiv [x_i, y_i, z_i]$ in the coordinate system $S_i(O_i, X_i, Y_i, Z_i)$, if you know the definition of his position $A \equiv [x_{i+1}, y_{i+1}, z_{i+1}]$ in the coordinate system $S_{i+1}(O_{i+1}, X_{i+1}, Y_{i+1}, Z_{i+1})$ and if the coordinate system given the previous coordinate system $S_i(O_i, X_i, Y_i, Z_i)$ performs any of the possible movements listed in the fifth rule.

In monograph [11] the fundamental mathematical relationships for the modeling of working accuracy of machine tools are derived with a serial kinematic structure of general shape. The mathematical model of the ideal tool trajectory is in the form of a matrix equation:

$$\{\mathbf{r}_0(t)\} = \left(\prod_{i=1}^n [\mathbf{R}_{i,i-1}(t)] \right) \{\mathbf{r}_n\} + \sum_{i=1}^{n-1} \left(\left(\prod_{j=1}^i [\mathbf{R}_{j,j-1}(t)] \right) (\{\mathbf{T}_{i+1,i}(t)\} + \{\mathbf{K}_{i+1,i}\}) \right) + \{\mathbf{T}_{10}(t)\} + \{\mathbf{K}_{10}\} \quad (1)$$

where $\{\mathbf{r}_0(t)\}$ is the tool contact point position vector in the workpiece coordinate system (model body T_0),

$\{\mathbf{r}_n\}$ is the tool contact point position vector in the tool carrier coordinate system (model body T_n),

$\{\mathbf{R}_{j,j-1}(t)\}$ is the rotational motion transformation matrix of the model body T_i relative to the T_{i-1} model body,

$\{\mathbf{T}_{i+1,i}(t)\}$ is the linear motion transformation vector of the model body T_{i+1} relative to the T_i model body,

$\{\mathbf{K}_{i+1,i}\}$ is the starting position vector of the model body T_{i+1} coordinate system in the T_i model body coordinate system,

t is the time.

The final machining inaccuracy is determined by the sum of part deformation due to production forces and position inaccuracy of all model bodies (machine nodes) from tool to workpiece in a coordinate system of workpiece in time t that in mathematical language could be written in a form [12].

$$\{\Delta(t)\} = \{\Delta_0(t)\} + \sum_{i=1}^n \left(\left(\prod_{j=1}^i [\mathbf{R}_{j,j-1}(t)] \right) (\{\delta_i(t)\} + [\boldsymbol{\varepsilon}_i(t)] \{\mathbf{r}_i(t)\} \right), \quad (2)$$

where the vector of deformations of the machined part is

$$\{\Delta_0(t)\} = \{\delta_0(t)\} + [\boldsymbol{\varepsilon}_0(t)] \{\mathbf{r}_0(t)\} \quad (3)$$

and the vectors

$$\{\Delta_i(t)\} = \{\delta_i(t)\} + [\boldsymbol{\varepsilon}_i(t)] \{\mathbf{r}_i(t)\} \quad (4)$$

represent the final position inaccuracies of active tool's point position caused by position inaccuracies of individual model bodies T_i expressed in the coordinate systems of these model bodies. The second part of Eq. (2) therefore represents a summary position inaccuracy of the active tool's point that is caused by position inaccuracies of all model bodies T_i and is reflected in the workpiece coordinate system.

The vector of linear inaccuracies of model body T_i in Eq. (2) defined relationship

$$\{\delta_i(t)\} = \{\delta_{xi}(t) \delta_{yi}(t) \delta_{zi}(t)\}^T, \quad (5)$$

where $\delta_{xi}(t)$, $\delta_{yi}(t)$ and $\delta_{zi}(t)$ are linear inaccuracies in the direction of corresponding coordinate axes.

The matrix of angular inaccuracies of model body T_i is defined by the relationship

$$[\boldsymbol{\varepsilon}_i(t)] = \begin{bmatrix} 0 & -\psi_i(t) & v_i(t) \\ \psi_i(t) & 0 & -\phi_i(t) \\ -v_i(t) & \phi_i(t) & 0 \end{bmatrix}, \quad (6)$$

where $\phi_i(t)$, $v_i(t)$ and $\psi_i(t)$ are angular inaccuracies (rotations about the axes X_i , Y_i , Z_i).

The position vector of active tool's point in coordinate system of model body T_i – vector $\mathbf{r}_i(t)$ in Eqs. (2) and (4) is defined by the relationship

$$\begin{aligned} \{\mathbf{r}_i(t)\} &= \left(\prod_{j=i}^{n-1} [\mathbf{R}_{j+1,j}(t)] \right) \{\mathbf{r}_n\} \\ &+ \sum_{j=i}^{n-2} \left(\left(\prod_{k=i}^j [\mathbf{R}_{k+1,k}(t)] \right) (\{\mathbf{T}_{j+2,j+1}(t)\} + \{\mathbf{K}_{j+2,j+1}\}) \right) + \{\mathbf{T}_{i+1,i}(t)\} \\ &+ \{\mathbf{K}_{i+1,i}\} \end{aligned} \quad (7)$$

Virtual machining with thinking of acting forces calculating the inaccuracies of the position of all model bodies in the corresponding $t \in \langle O; T \rangle$ is mathematically defined by Eqs. (2)–(6). The result is a mathematical model of the real machined surface in the form of vector function

$$\mathbf{f}(t) = \mathbf{r}_0(t) + \mathbf{\Delta}(t). \quad (8)$$

3. Practical example

Practical implementation of the virtual machining on the virtual machine tool model is represented by the example of a virtual model of a machining centre with a horizontal spindle axis for machining non-rotating components, the design of which stems from the Box-in-Box concept and is complemented by a rotary table with the relevant construction dimensions (**Table 1**). This can be considered in a simplified

Dimension	a	b	B_4	B_5	h	h_3	h_4	h_5
Value (mm)	120	235	300	300	72	20	20	62
Dimension	H_3	H_4	H_5	L_2	L_3	L_4	L_5	p
Value (mm)	134	200	700	300	750	760	380	66

Table 1.
 Design dimensions of the horizontal machining centre.

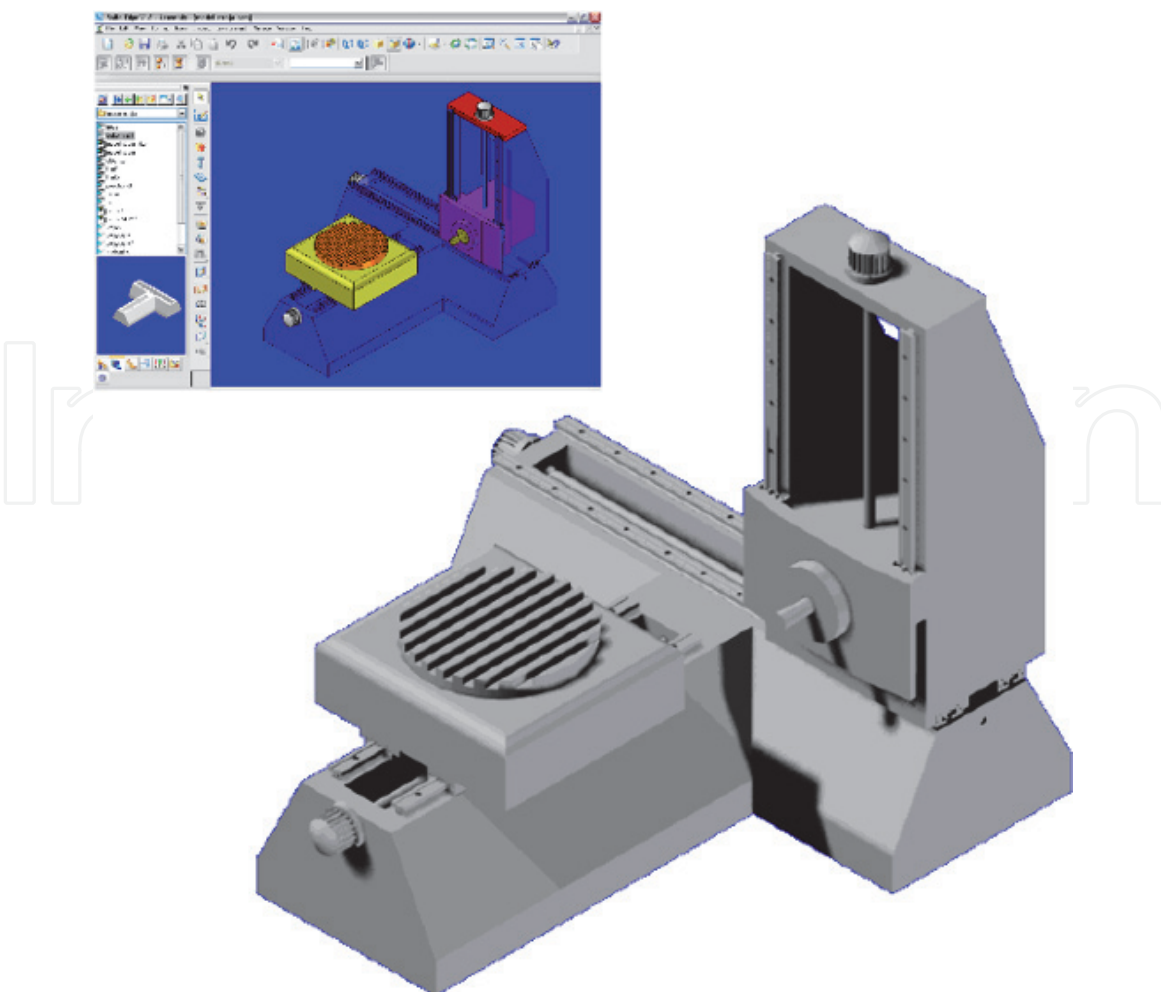


Figure 1.
 Virtual model of the machining Centre.

version as a simple “indexing” table (allowing positioning of the workpiece for example by 90°) or as a variant with a controlled axis B (allowing machining when the workpiece is rotated about the vertical axis continuously).

The proposed machine (see **Figure 1**) has a work area defined by the maximum workpiece dimensions $L_{omax} = 600$ mm, $B_{omax} = 500$ mm a $H_{omax} = 600$ mm. The simplified machine model is illustrated in **Figure 2** and consists of the following

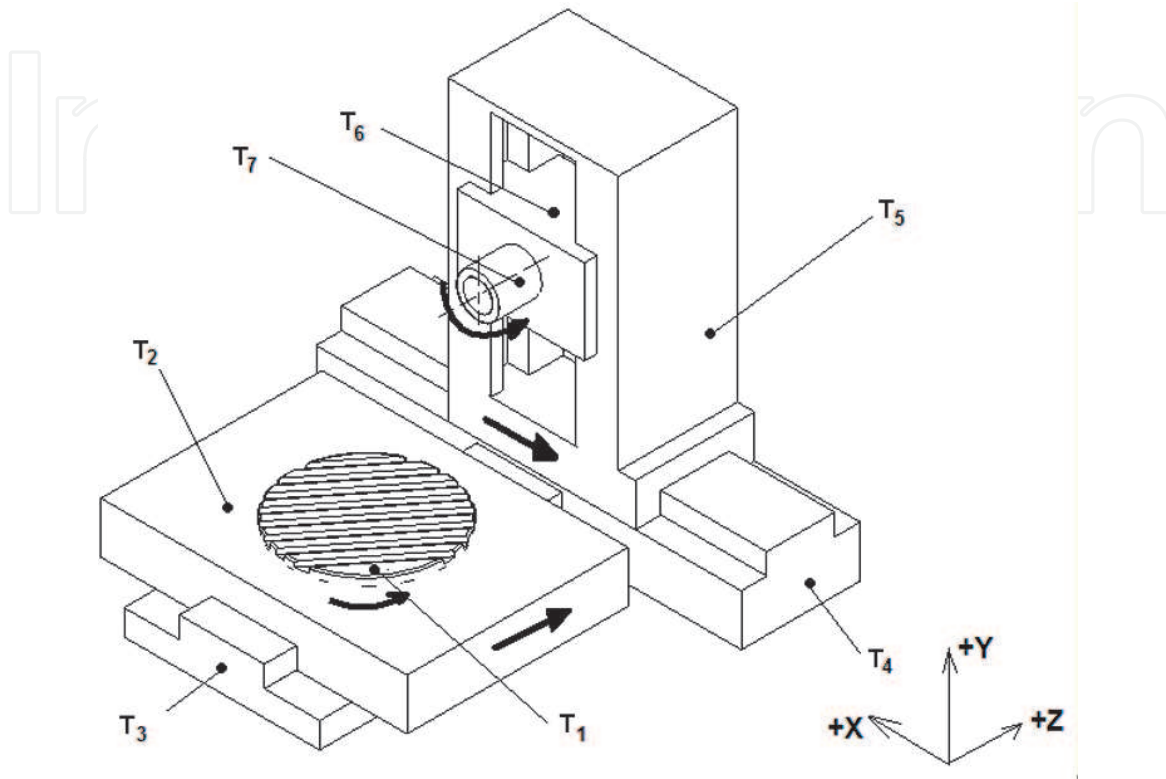


Figure 2.
Simplified computational model of the machining Centre with rotary table.

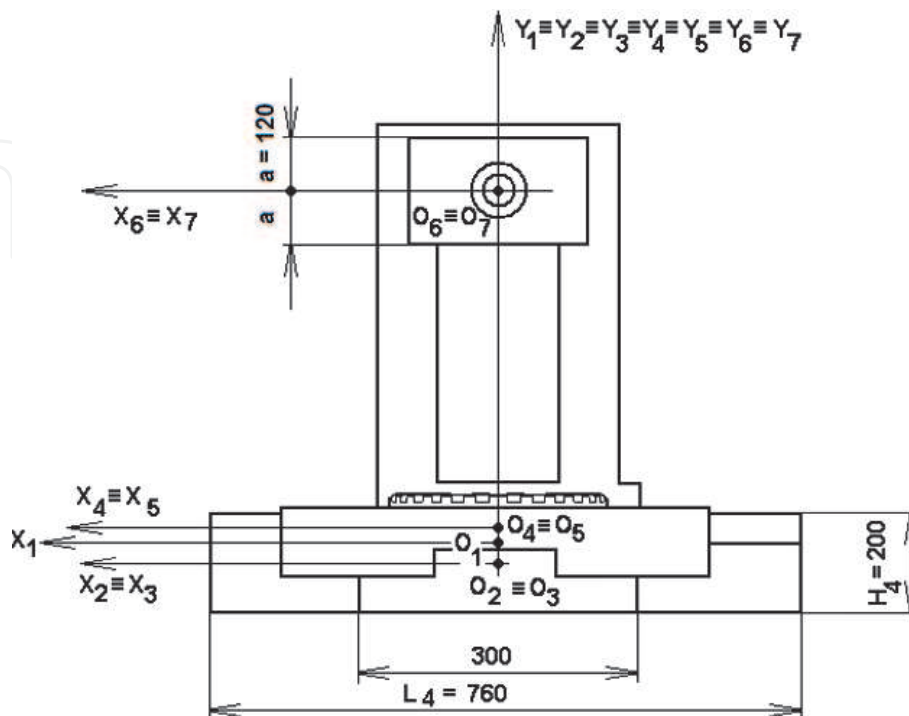


Figure 3.
Detailed computational model of the machining centre with rotary table (front view).

model bodies (gradually from the workpiece towards the tool): T_1 , rotary table; T_2 , table; T_3 , bed (longitudinal part); T_4 , bed (transverse part); T_5 , stand; T_6 , head-stock; and T_7 , spindle. The illustration also shows the basic layout of the machine's coordinate system. A detailed dimensional computational model of the machining centre is shown in **Figures 3–5**.

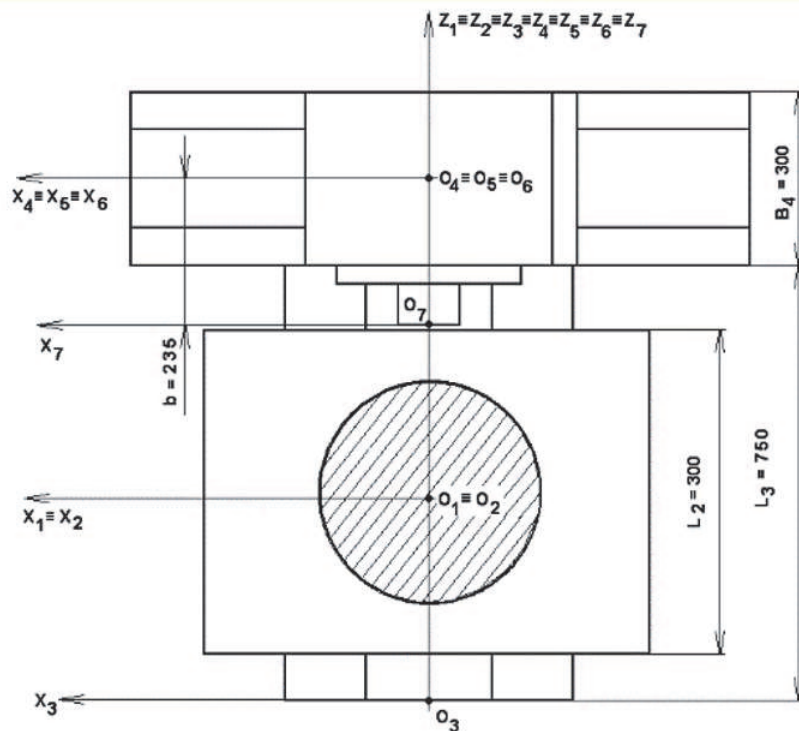


Figure 4.
 Detailed computational model of the machining centre with rotary table (ground plan).

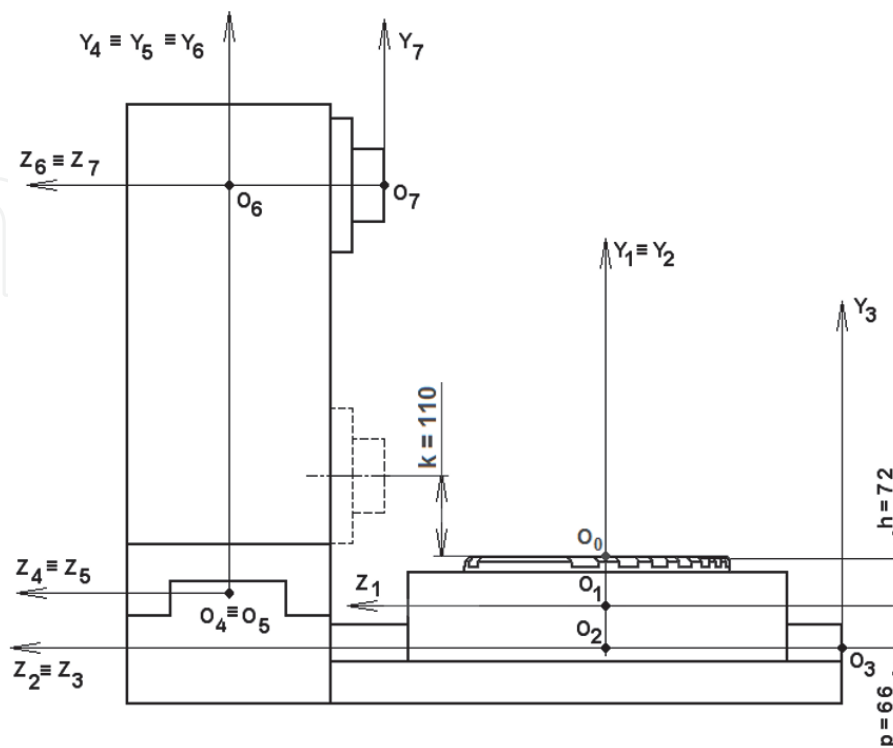


Figure 5.
 Detailed computational model of the machining centre with rotary table (side view).

The stand: $[\mathbf{R}_{54}(t)]$, $\{\mathbf{T}_{54}(t)\}$, $\{\mathbf{K}_{54}\}$.

The bed—transverse part: $[\mathbf{R}_{43}(t)]$, $\{\mathbf{T}_{43}(t)\}$, $\{\mathbf{K}_{43}\}$.

The bed—longitudinal part: $[\mathbf{R}_{32}(t)]$, $\{\mathbf{T}_{32}(t)\}$, $\{\mathbf{K}_{32}\}$.

The longitudinal table: $[\mathbf{R}_{21}(t)]$, $\{\mathbf{T}_{21}(t)\}$, $\{\mathbf{K}_{21}\}$.

The rotary table: $[\mathbf{R}_{10}(t)]$, $\{\mathbf{T}_{10}(t)\}$, $\{\mathbf{K}_{10}\}$.

The virtual workpiece was designed as a quad shape body with dimensions $L_o = 450$ mm, $B_o = B_{o\max} = 500$ mm and $H_o = H_{o\max} = 600$ mm. The position of the workpiece on the table is symmetrical, and the vertical planes of symmetry of the workpiece and the table are identified.

In virtual machining, the simultaneous machining of two vertical planar faces of the workpiece by the front and cylindrical peripheral surfaces of the tool—the front cylindrical cutter—was considered. It is considered an unsymmetrical down-milling. The tool will be the front cylindrical milling cutter R215.59–06, the diameter $d_f = 20$ mm and the number of teeth $z_f = 4$. Milling depth $h_f = 10$ mm, milling width b_f is equal to half the diameter of the cutter d_f , machining with motion of the headstock (direction Y) is from the top down, feed rate $f_Y = 0.09$ mm (feed rate on the milling tooth), cutting speed $v_c = 170$ m·min⁻¹, and spindle speed is adjusted to $n_v = 2700$ min⁻¹. When looking from the machine stand to the workpiece, we cut the front of the workpiece over the entire height machining starting from the top right corner of the workpiece (see **Figures 6** and **7**).

4. Virtual machining result

The machining of the respective planar faces of the workpiece by the front cylindrical milling cutter begins at the coordinate $y_o(0) = 590$ mm and ends at $y_o(T) = k = 110$ mm, resulting from the construction of the headstock and spindle. Thus, the headstock travel at time T is 480 mm, with the total machining process lasting at selected feed rates, and the number of milling teeth and spindle speed $T = 480/16.2 \approx 29.63$ s. If we divide the total machining time into, for example, 10 equal sections, $\Delta t = 2.963$ s; the headstock path is simultaneously divided into 10 equal sections of 48 mm in length. In these positions of the headstock, the corresponding numerical simulations are performed.

The power ratios for machining (see **Figure 8**) were simulated on the basis of the structural equation for the tangential component of the cutting force (cutting resistance) according to [13]

$$F_c = 682 h_f^{0.86} b_f z_f f_Y^{0.72} d_f^{-0.86} \text{ (N)} \quad (9)$$

where the appropriate dimensions are set in millimetres (mm). On the basis of Eq. (9), according to [13], the components of the cutting force (cutting resistance) in the directions of the individual coordinate axes are valid for asymmetrical down-milling:

$$\left. \begin{aligned} F_X &= (0.60 \div 0.90) F_c \\ F_Y &= (0.45 \div 0.70) F_c \\ F_Z &= (0.50 \div 0.55) F_c \end{aligned} \right\}, \quad (10)$$

Due to the proportions of the design of the individual model bodies of the machine, only the deformations of the stand were considered in the other calculations. For numerical simulations, relationships (10) were used for the most

unfavourable values; therefore, the respective components of the cutting forces (resistances) are for down-milling:

$$\left. \begin{aligned} F_X &= 0.90 F_c = 3386.0563 \text{ N} \approx 3386 \text{ N} \\ F_Y &= 0.70 F_c = 2633.5993 \text{ N} \approx 2634 \text{ N} \\ F_Z &= 0.55 F_c = 2069.2566 \text{ N} \approx 2070 \text{ N} \end{aligned} \right\}, \quad (11)$$

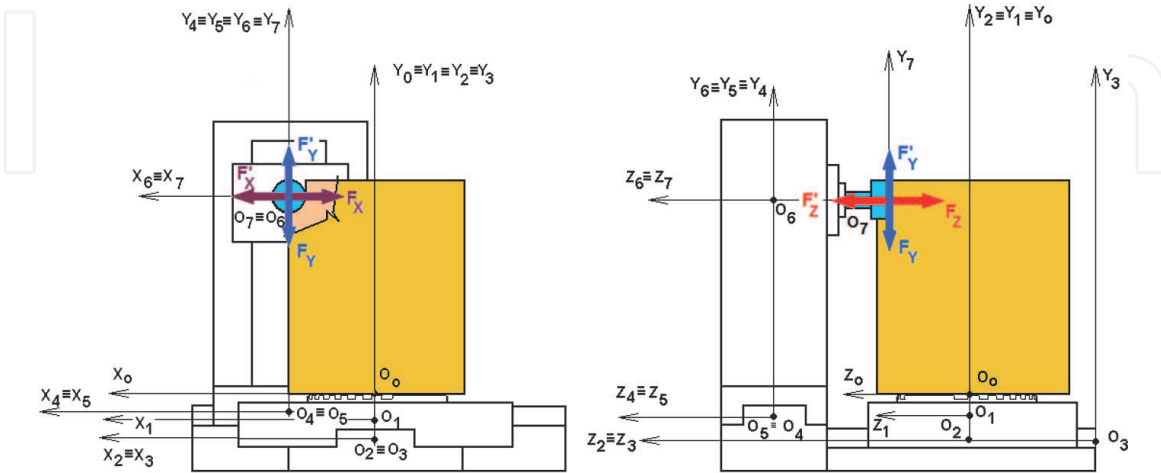


Figure 8.
Layout of cutting forces and resistances for virtual machining.

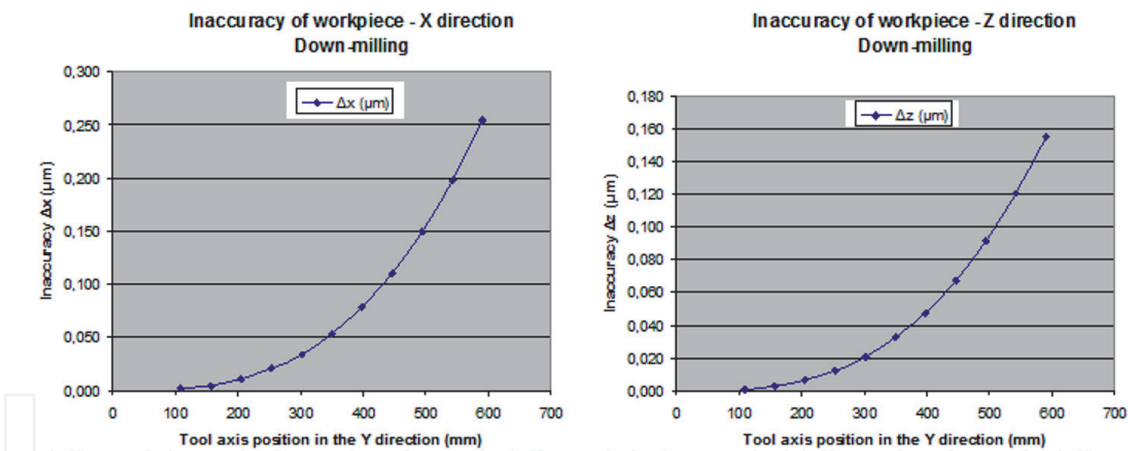


Figure 9.
Graphical representation of workpiece inaccuracies.

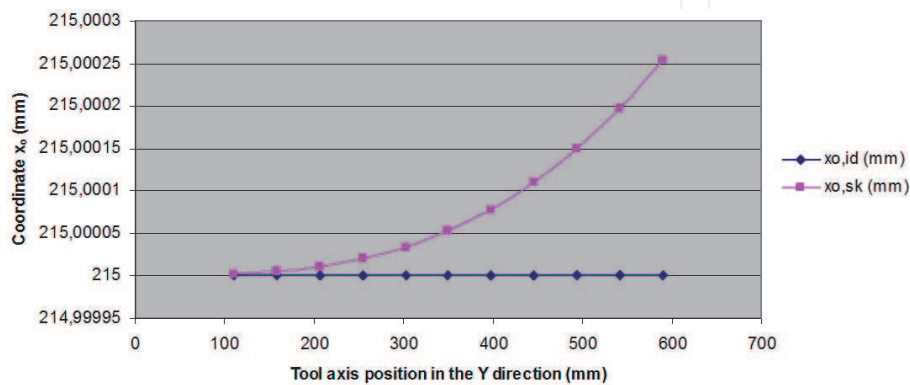


Figure 10.
The real coordinates of the machined surface in X direction by down-milling.

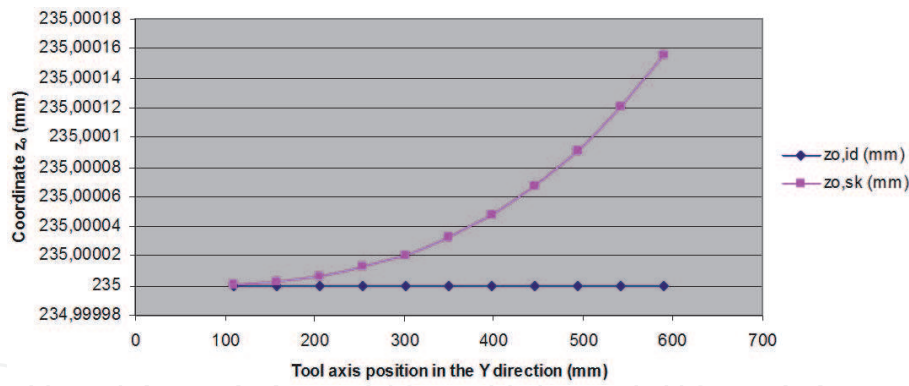


Figure 11.
 The real coordinates of the machined surface in Z direction by down-milling.

Position of the headstock i	Down-milling							
	t	$y_{oi}(t)$	$\Delta x_{oi}(t)$	$x_{0ib} \dot{i}_d(t)$	$x_{0ibsk}(t)$	$\Delta z_{oi}(t)$	$z_{0bid}(t)$	$z_{0ibsk}(t)$
	(s)	(mm)	(μm)	(mm)	(mm)	(μm)	(mm)	(mm)
1	0	590	0.254	215	215.00025	0.155	235	235.00016
2	2963	542	0.197	215	215.00020	0.120	235	235.00012
3	5926	494	0.149	215	215.00015	0.091	235	235.00009
4	8889	446	0.110	215	215.00011	0.067	235	235.00007
5	11.852	398	0.078	215	215.00008	0.048	235	235.00005
6	14.815	350	0.053	215	215.00005	0.032	235	235.00003
7	17.778	302	0.034	215	215.00003	0.021	235	235.00002
8	20.741	254	0.020	215	215.00002	0.012	235	235.00001
9	23.704	206	0.011	215	215.00001	0.007	235	235.00001
10	26.667	158	0.005	215	215.00000	0.003	235	235.00000
11	29.63	110	0.002	215	215.00000	0.001	235	235.00000

Table 2.
 Virtual machining results with down-milling.

Some results of numerical experiments are shown in **Figures 9–11**; numerical values are given in **Table 2**.

5. Experimental measurement of milling machine stiffness during X-axis positioning

Inspiration to modify the commonly used extended static stiffness measurement method resulted from the significantly different experimentally measured static stiffness values of the new loading method compared to the standard stiffness measurement method. Static stiffness measurements in this experiment were performed under the axis load immediately after reaching the desired position. From the known force and deflection, it is possible to determine the stiffness of the table relative to the base at a given programmed linear unit position. Thus, the stiffness measurement results more faithfully reflect the actual ratios that occur during machining. This note is important in that relatively slow changes, such as a

change in the thickness of the oil layer in the contact surfaces, may occur after the movement has stopped, which may affect the static stiffness.

An important observation from the measurements is that the measured static stiffness of the table greatly depended on the previous operation of the table and the way it was loaded. The classical stiffness measurement showed up to three times higher stiffness values than the modified method using identical tools and conditions. The reasons for such a considerable difference in stiffness are given by the structural arrangement and the effect of nonlinearities on the contact surfaces of the cross-table components. During the measurement, all machine parts were stationary. This modified view of the static stiffness can be used to change the design philosophy of the machine tool. This is applicable in engineering practice, especially in the field of machine tool design, which will ensure higher machining accuracy under comparable conditions. In the experiments performed, the Renishaw XL80 laser interferometer was used to measure deformation and displacement. Measuring accuracy of the manufacturer guarantees better than $0.5 \mu\text{m/m}$.

5.1 Arrangement of experiments

For experimental static stiffness measurement, the Kondia B 640 CNC Vertical Milling Machine was used as a production machine with three fully controlled axes [14].

5.1.1 First experiment: gradual loading of table positions

During gradual loading of table positions, the work procedure consisted of alternating cycles with and without the load. The reason for such a procedure was to estimate the thermal expansion of the table against the base during one cycle. One cycle consisted of the table's gradual positioning of nine positions in the X axis (**Figure 12**). Using the laser interferometer, an exact position was measured.

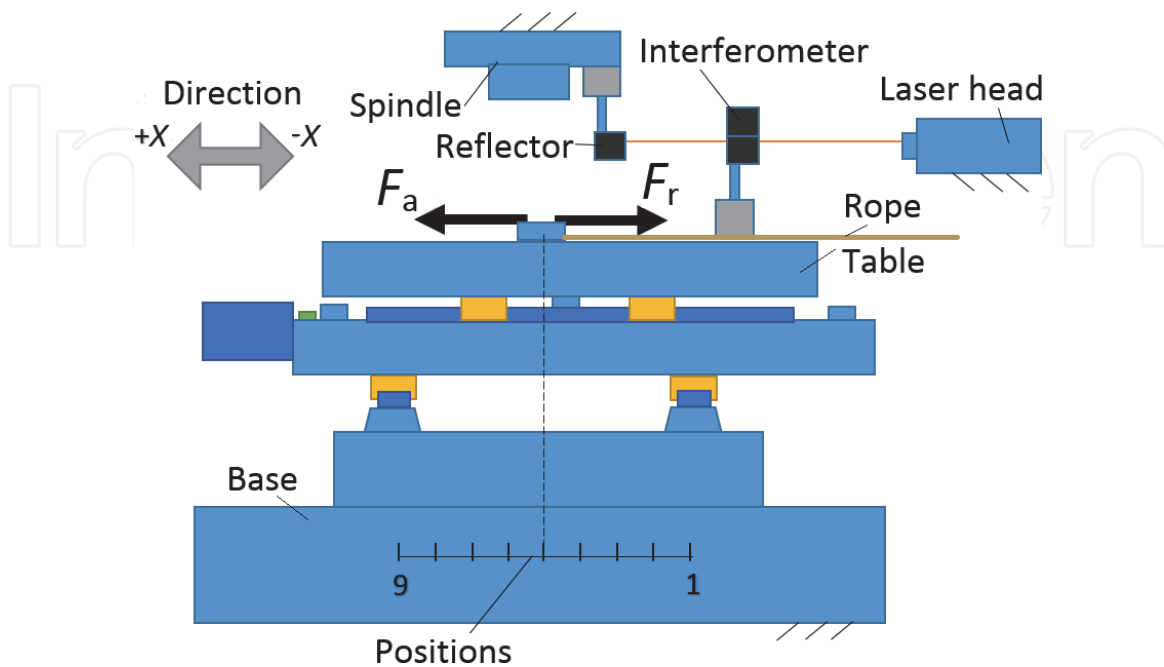


Figure 12. Measurement sequencing in direction of the X axis on the cross-milling table.

From this, stiffness was determined in each position in both directions of the table starting with the given position (**Figure 13**). At each position, the average offset from the slope can be calculated.

As shown, the stiffness measured by this method is approximately the same in either direction. The highest stiffness was detected around position 8. This fact is consistent with the machine design since the lowest matrix and motor distance is at this position (**Figure 12**). The screw in this position is least involved in the stiffness deterioration.

5.1.2 Second experiment: static loading of table positions

The static loading of the table was performed to verify the continuous loading method. The working procedure consisted of moving the table to the measured position. In the given position, it was gradually loaded and relieved by the F_r force. In each position, the loading and unloading cycle was repeated twice. The reason was that only at the second cycle the backlash from the load was determined in the given direction. The stiffness of the system has been determined from the charted slope (**Figure 14**). This method of stiffness measurement can practically be considered a classic one.

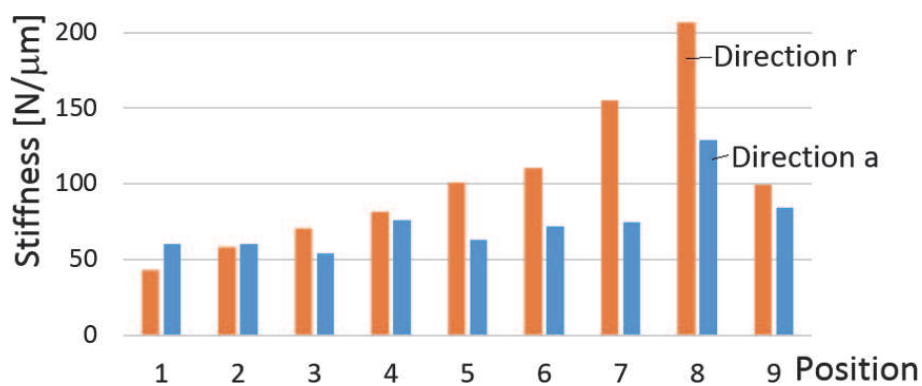


Figure 13. Measured stiffness of the shift in the a and r directions, respectively.

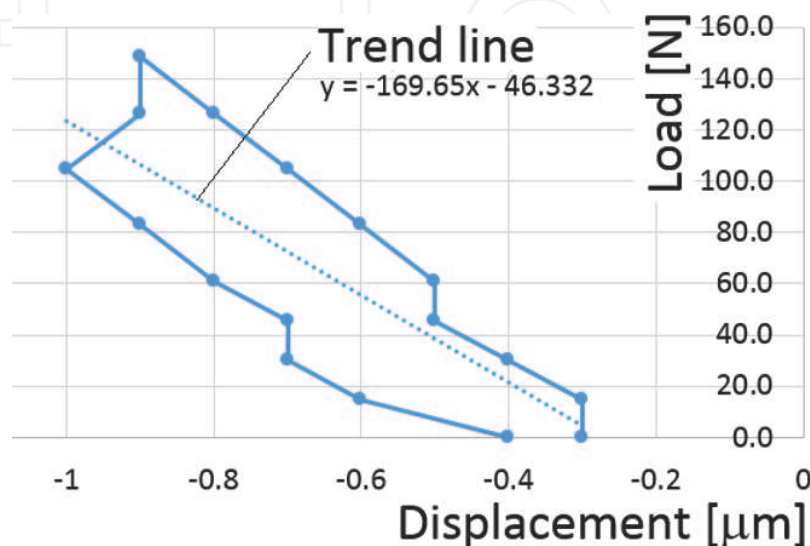


Figure 14. Stiffness measurement in position 8 (second loading). The slope shows stiffness (169 N/μm).

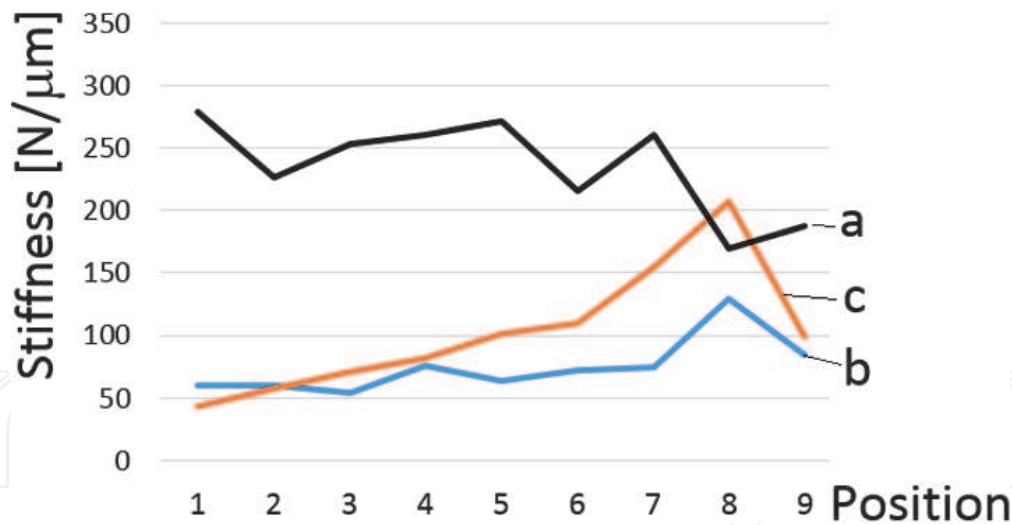


Figure 15. Size comparison of (a) the static stiffness, (b) the shift stiffness in direction a and (c) the shift stiffness in direction r.

The course of static stiffness in individual positions is shown in **Figure 15**. The resulting course was compared with the results of the first experiment. As the graph clearly shows, the static stiffness is considerably different from the shift stiffness.

6. Discussion

As the experiments show, the actual position of the table depends on the previous method of loading. Immediate static load can only be given a partial credit for the assumed position. This fact places special demands on how to compose a mathematical model. In common mathematical models, the input values translate into a clear result. This is not the case. For that reason, we did not proceed with creating the mathematical model. Only a schematic model has been created (**Figure 16**) [14].

The basis of the model is the source of resistance to movement. These are friction, deformation of the contact surfaces and elastic deformation of the machine

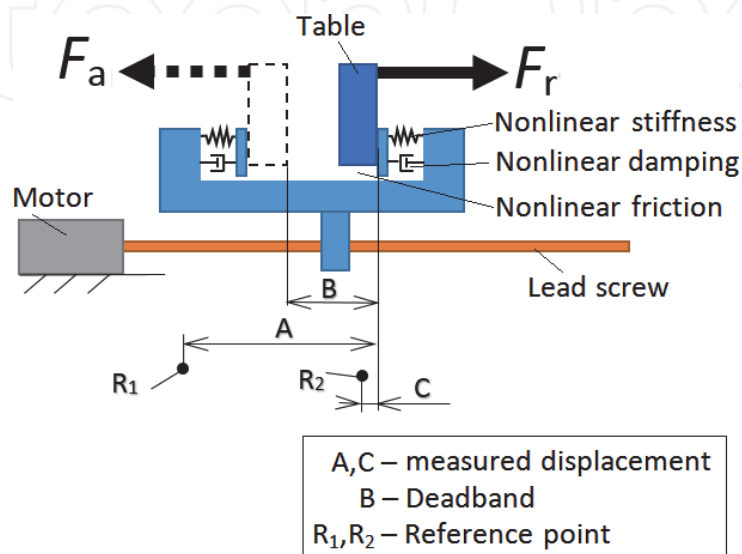


Figure 16. Machine positioning model.

structure. All three sources cause nonlinearity between the load and the position change.

As follows from the experiments, the classic machine stiffness measurement does not detect design deficiencies in terms of drive quality and the machine's alignment. The measured stiffness values are in the order of three times the values measured when the machine is shifted to the measured position. Yet, the method of shifting the movable parts under load clearly reflects the real state during machining better.

The stiffness analysis shows that if the load direction is not changed, the stiffness will be higher. This is related to the definition of the backlash and the direction of the previous load in the individual parts of the machine.

The purpose of the construction of the mathematical model is based on the idea of improving the design of the machine in terms of work accuracy of production. There are two possible procedures. The first is to minimise the adverse effect of nonlinearities in the construction nodes. This can be achieved, for example, by selecting preloaded connections, reducing the number of kinematic elements to a minimum and the like. The second procedure is control of nonlinear states. This procedure requires feedback that is provided by sensors, for example, temperature, vibration sensors and force and deflection sensors. The last two sensors can be used to the stiffness measure of the measured point at a given time and space.

Theoretically, there is no analytical method for calculating nonlinearities. For the first time, French mathematician Henri Poincaré demonstrated it in the task of solving the movement of the three heavenly bodies (three body problem) at the end of the nineteenth century. However, the awareness of this fact was very gradual. It was not until the development of computer technology and chaos theory in the 1970s of the last century that nonlinear problems began to be solved by numerical simulation. Such a nonlinear model gives a solution, but the trajectory of the output functions is uncertain. It moves with some probability that the result is in some interval. The system works very much like the weather forecast.

7. Conclusion

The stiffness measurement by laser interferometer opens up new possibilities of evaluation, not exactly feasible under classic measurement with dial micrometre indicators. The results obtained by measurements point to the fact that the static stiffness depends both on the previous method of loading and the direction of the start of the measured position. The proposed shift stiffness measurement methodology allows for a better assessment of the machine's working ability. It also allows for the detection of faults caused by, for example, incorrect assembly of machine components. The method also points to structural design deficiencies that would not be detectable from a classic stiffness measurement.

The comparison of the theoretical inaccuracy resulting from the design of the machine components to some extent is also related to the experimental results of the measurement of the static stiffness at different axis positions. Experiments show that the stiffness change is also related to the location of the nut and bolt (**Figure 13**, position 8). This is the influence of design accuracy, which was theoretically described in the introductory chapters. In addition, the previous working action and the amount of load, which is also a design matter, also affect the stiffness and hence the accuracy. However, there are many nonlinear elements in this field, so the construction of a reliable mathematical model is considerably limited. When designing the design of good machines, it is advisable to keep these effects in mind.

Acknowledgements

This work was supported by the Slovak Research and Development Agency under the Contract no. APVV-18-0413: Modular architecture of structural elements of production machinery.

IntechOpen

IntechOpen

Author details

Peter Demeč and Tomáš Stejskal*
Department of Manufacturing Machinery, Faculty of Mechanical Engineering,
Technical University of Košice, Košice, Slovakia

*Address all correspondence to: tomas.stejskal@tuke.sk

IntechOpen

© 2020 The Author(s). Licensee IntechOpen. This chapter is distributed under the terms of the Creative Commons Attribution License (<http://creativecommons.org/licenses/by/3.0>), which permits unrestricted use, distribution, and reproduction in any medium, provided the original work is properly cited. 

References

- [1] Chen XB, Geddam A, Yuan ZJ. Accuracy improvement of three-axis CNC machining centers by quasi-static error compensation. *Journal of Manufacturing Systems*. 1997;**16**(5): 323-336
- [2] Lin M-T, Shih-Kai W. Modeling and improvement of dynamic contour errors for five-axis machine tools under synchronous measuring paths. *International Journal of Machine Tools and Manufacture*. 2013;**72**:58-72
- [3] Mayr J et al. Comparing different cooling concepts for ball screw systems. *Proceedings of ASPE Annual Meeting*; 2010
- [4] Mayr J et al. Thermal issues in machine tools. *CIRP Annals - Manufacturing Technology*. 2012;**61.2**: 771-791
- [5] Brecher Chr, Wissmann A. Modelling of thermal behaviour of a milling machine due to spindle load. *12th CIRP Conference on Modelling of Machining Operations*. Vol. 2; 2009
- [6] Wang Y. et al. compensation for the thermal error of a multi-axis machining center. *Journal of Materials Processing Technology*. 1998;**75**(1):45-53
- [7] Donmez MA, Hahn M-H, Soons JA. A novel cooling system to reduce thermally-induced errors of machine tools. *CIRP Annals - Manufacturing Technology*. 2007; **56**(1):521-524
- [8] Gebhardt M et al. High precision grey-box model for compensation of thermal errors on five-axis machines. *CIRP Annals - Manufacturing Technology*. 2014;**63.1**:509-512
- [9] Huang DT-Y, Lee J-J. On obtaining machine tool stiffness by CAE techniques. *International Journal of Machine Tools and Manufacture*. 2001; **41.8**:1149-1163
- [10] Altintas Y et al. Virtual machine tool. *CIRP Annals - Manufacturing Technology*. 2005;**54**(2):115-138
- [11] Demeč P, Svetlík J. *Virtual Prototyping of Machine Tools*. 1st ed. RAM-Verlag: Lüdenscheid; 2017. p. 158. ISBN 978-3-942303-61-3
- [12] Demeč P, Svetlík J. Virtual machining and its experimental verification. *Acta Mechanica Slovaca*. 2009;**13**(4):68-73
- [13] Lipták O et al. *Production Technology - Machining*. 1st ed. Bratislava: ALFA; 1979. (in Slovak)
- [14] Stejskal T, Svetlík J, Dovica M, Demeč P, Král' J. Measurement of static stiffness after motion on a three-axis CNC milling table. *Applied Sciences*. 2018;**8**(1):15. DOI: 10.3390/app8010015